Water Research 185 (2020) 116226

Contents lists available at ScienceDirect

Water Research

journal homepage: www.elsevier.com/locate/watres

Kinetic modeling of the synergistic thermal and spectral actions on the inactivation of *Cryptosporidium parvum* in water by sunlight

Ángela García-Gil[a], María Jesús Abeledo-Lameiro[b,c], Hipólito Gómez-Couso[b,c], Javier Marugán[a,*]

[a] Department of Chemical and Environmental Technology (ESCET), Universidad Rey Juan Carlos, C / Tulipán s/n, 28933 Móstoles, Madrid, Spain
[b] Department of Microbiology and Parasitology, Faculty of Pharmacy, University of Santiago de Compostela, Campus Vida, 15782 Santiago de Compostela, A Coruña, Spain
[c] Research Institute on Chemical and Biological Analysis, University of Santiago de Compostela, 15782 Santiago de Compostela, A Coruña, Spain

ARTICLE INFO

Article history:
Received 11 May 2020
Revised 20 July 2020
Accepted 23 July 2020
Available online 23 July 2020

Keywords:
Solar water disinfection (SODIS)
Household water treatment (HWT)
Protozoa inactivation
Quantum yield
Extinction coefficient
Water temperature

ABSTRACT

Water contamination with the enteroprotozoan parasite *Cryptosporidium* is a current challenge worldwide. Solar water disinfection (SODIS) has been proved as a potential alternative for its inactivation, especially at household level in low-income environments. This work presents the first comprehensive kinetic model for the inactivation of *Cryptosporidium parvum* oocysts by sunlight that, based on the mechanism of the process, is able to describe not only the individual thermal and spectral actions but also their synergy. Model predictions are capable of estimating the required solar exposure to achieve the desired level of disinfection under variable solar spectral irradiance and environmental temperature conditions for different locations worldwide. The thermal contribution can be successfully described by a modified Arrhenius equation while photoinactivation is based on a series-event mechanistic model. The wavelength-dependent spectral effect is modeled by means of the estimation of the *C. parvum* extinction coefficients and the determination of the quantum yield of the inactivation process. Model predictions show a 3.7% error with respect to experimental results carried out under a wide range of temperature (30 to 45 °C) and UV irradiance (0 to 50 $W \cdot m^{-2}$). Furthermore, the model was validated in three scenarios in which the spectral distribution radiation was modified using different plastic materials common in SODIS devices, ensuring accurate forecasting of inactivation rates for real conditions.

1. Introduction

Water contamination with the enteropathogen *Cryptosporidium* is a universal challenge (Efstratiou et al., 2017; Hamilton et al., 2018; Hofstra and Vermeulen, 2016; Karanis et al., 2007). Based on WHO reports (WHO, 2015), there were approximately 64 million of estimated cases of illness caused by *Cryptosporidium* and 35% of them were related to contact with contaminated water sources. Moreover, cryptosporidiosis has a worldwide distribution. In developed countries, prevalence rates range from 0.3 to 54.2%, mainly related to recreational or drinking water (Abeywardena et al., 2015), and reported because of the existence of surveillance systems for routine detection of *Cryptosporidium* (Cacciò and Putignani, 2014). Furthermore, water bodies may also be contaminated by sewage or effluents from wastewater treatment plants (WWTP), whose treatments are insufficient to achieve the total removal of *Cryptosporidium* oocysts (Nasser, 2016; Vermeulen et al., 2019). However, the prevalence is assumed to be higher in developing countries (Putignani and Menichella, 2010). In these regions, *Cryptosporidium* is one of the top three pathogens causing diarrheal disease in children under two years old, and it is responsible for 30–50% of childhood mortality (Kotloff et al., 2013) estimated in 455,000 deaths in Sub-Saharan region (Sow et al., 2016).

The risk of infection by *Cryptosporidium* through drinking water can be reduced by key intervention methods, such as appropriate selection and protection of the catchment and the installation of an effective filtration step and disinfection by UV-C (Betancourt and Rose, 2004; Swaffer et al., 2018). However, developing countries cannot afford the use of advanced technologies and demand low-cost water disinfection processes. Solar water disinfection (SODIS) is a low-cost, easy-to-use and sustainable process to conduct water treatment at the household level. This process is especially interesting for countries where high solar doses are received all around the year. This process, commonly carried out by the expo-

* Corresponding author.
E-mail address: javier.marugan@urjc.es (J. Marugán).

https://doi.org/10.1016/j.watres.2020.116226

sure to sunlight of 2 L polyethylene terephthalate (PET) bottles for 6 h, is based on the harmful damage of the UV solar radiation and high temperatures on microorganisms and has been successfully tested for the removal of viruses, bacteria, and protozoa, including *Cryptosporidium parvum* (Wegelin et al., 1994; McGuigan et al., 2012; Gómez-Couso et al., 2012, 1998). At present, SODIS is one of the recommended methods for disinfection of household drinking water (WHO/UNICEF, 2005).

Solar inactivation of *C. parvum* in pure water is dominated by direct endogenous damage caused by UV-B absorption by genome, since the *C. parvum* action spectrum resembles that of the DNA absorption (Busse et al., 2019; Liu et al., 2015). This similarity also confirms the wavelength dependence for the photoinactivation of *C. parvum* oocysts (Beck et al., 2015; Busse et al., 2019; Linden et al., 2001). Recently, Busse et al. (2019) applied the series-event model (Severin et al., 1983), that assumes stepwise units of damage until a threshold amount is accumulated, to obtain the relative inactivation constant as a function of wavelength. Actually, the spectral dependence suggests the interest of the potential substitution of PET for other SODIS container materials with higher UV-B transmittance (García-Gil et al., 2020a).

This work describes for the first time the kinetic modeling of the synergistic effect of the photonic and thermal effects on the inactivation of *C. parvum* oocysts. The developed model provides an accurate estimation of the required exposure time for the solar inactivation of this protozoon depending on the radiation intensity, available spectral range and water temperature. Application of the model predictions allows the calculation of SODIS treatment time needed to provide safe drinking water from the protozoan point of view, whose higher resistance also ensures the elimination of other less resistant waterborne pathogens.

2. Materials and methods

2.1. Cryptosporidium parvum oocysts

Cryptosporidium oocysts were collected from a naturally infected neonatal Friesian-Holstein calf. Concentration (0.04 M phosphate-buffered saline [PBS] pH 7.2 and diethyl ether), purification (discontinuous caesium chloride gradients), quantification (Neubauer haemacytometer) and molecular characterization were performed as previously reported (Gómez-Couso et al., 2012). Briefly, feces were collected from a calf by rectal sampling and stored at 5 °C. Fecal material was then homogenised in 10–20 mL of PBS (0.04 M, pH 7.2), filtered through two sieves (mesh sizes 150 and 45 μm), shaken with diethyl ether (2:1, v/v) and concentrated by centrifugation at 2000 × *g*, for 15 min, at 4 °C. The resulting uppermost two layers were removed carefully and discarded, and the sediment was washed with PBS (0.04 M, pH 7.2) by centrifugation at 2000 × *g* for 15 min at 4 °C. *Cryptosporidium* oocysts were purified on discontinuous caesium chloride gradients of 1.05, 1.10 and 1.40 g·mL^{-1} by centrifugation at 2000 × *g* for 30 min at 4 °C. Finally, the oocysts were counted in a modified Neubauer haemocytometer, with 0.16% malachite green solution as counterstain (Kilani and Sekla, 1987; Lorenzo-Lorenzo et al., 1993). The isolate was identified as *C. parvum* by PCR amplification and sequence analysis of $a \approx$ 587-bp fragment of the small subunit rDNA gene (SSUrDNA) (Ryan et al., 2003).

2.1.1. Viability assays

The viability of *C. parvum* oocysts was determined by inclusion/exclusion of the fluorogenic vital dye propidium iodide (PI) and a further modification that includes an immunofluorescence antibody test to verify oocyst identification (Campbell et al., 1992; Dowd and Pillai, 1997). Briefly, 200 μL of the sediments were incubated with 15 μL of PI (Sigma-Aldrich, Co., St. Louis, Missouri, USA) working solution [1 mg·mL^{-1} in PBS (0.1 M, pH 7.2)] and 15 μL of monoclonal antibodies labelled with fluorescein isothiocyanate (FITC) (AquaGlo™ G/C Direct Test, Waterborne Inc., New Orleans, Louisiana, USA), at 37 °C, for 30 min (Gómez-Couso et al., 2012). Then, the samples were washed three times in PBS (0.04 M, pH 7.2) at 10,000 × *g*, for 5 min at room temperature. Oocysts were identified first under a FITC filter (excitation at 450–480 nm; barrier at 515 nm) before being examined for PI inclusion/exclusion under a PI filter (excitation at 510–550 nm; barrier at 590 nm). The proportions of ruptured (ghost), PI-positive (dead), and PI-negative (viable) oocysts were quantified in an epifluorescence microscope equipped with a Nomarski differential interference contrast, FITC and PI filters (Olympus AX70, Olympus Optical Co., Ltd., Tokyo, Japan). The results are shown as the concentration of PI-negative (viable) oocysts determined for each assay after triplicate counts of more than 100 oocysts.

2.2. Experimental design

Three sets of experiments were conducted. In the first set, experiments were carried out at different water temperatures (30, 40, 42, 43, 44, and 45 °C) in the dark to quantify the dark thermal inactivation of *C. parvum* oocysts. In the second set, inactivation experiments were performed using different UV irradiances (30, 40, and 50 W·m^{-2}) and water temperatures (30, 40, and 44 °C) to determine the contribution of the irradiance effect and its synergistic effect with water temperature. In the third set, experiments for the validation of the developed model predictions were carried out using plastic sheets placed between the illumination source and the water to test the wavelength dependence. Potential materials for the manufacture of SODIS containers (García-Gil et al., 2020a) were selected based on their different UV-B transmittances: polyethylene terephthalate (PET), polypropylene (PP) and polymethylmethacrylate (PMMA). For the three scenarios, three experiments were conducted: i) 50 W·m^{-2} of UV radiation and 30 °C of water temperature; ii) 50 W·m^{-2} and 44 °C; and, iii) 30 W·m^{-2} and 44 °C. Table S.1 shows the required treatment time to achieve 1-log reduction (90%) of *C. parvum* viability.

Experiments were carried out in a solar simulator (Atlas Suntest CPS+, ATLAS Material Testing Technology GmbH, Lisengericht, Germany) equipped with a 1100 W air-cooled xenon arc lamp and a combination of filters (Suprax, ATLAS, Material Testing Technology GmbH) to simulate the outdoor solar radiation spectrum. The irradiance was measured with a radiometer PMA2100 fitted with a PMA2107 digital non-weighted UV-*A*+*B* Sensor (280–400 nm) (Solar Light® Company, Inc, Glenside, Pennsylvania, USA). An open reaction-jacketed borosilicate beaker (135 × 75 mm) containing 400 mL of distilled water (pH 6.1, conductivity <10 µS·cm^{-1}, organic carbon <0.5 mg·L^{-1}) was spiked with 75,000 oocysts·mL^{-1} of *C. parvum* and exposed to artificial solar light at the established intensities of radiation and temperatures for a maximum exposure time of 6 h. The exterior of the reactor was completely black to avoid uncontrolled light reflections and guarantee that only the measured direct radiation participates in the process. In order to maintain the temperature of the water sample during the experiments, the reactor was connected to a refrigerated and heated bath circulator Fisherbrand™ Isotemp™ 4100 R20 (Thermo Fisher Scientific Inc., Waltham, Massachusetts, USA). Constant stirring of 250 rpm was kept during the experiments to ensure a homogeneous concentration of *C. parvum* oocysts. At different exposure times, 14 mL of the sample was removed and centrifuged at 2000 × *g*, 15 °C, for 15 min. The supernatant was discarded, and the sediment thus obtained was resuspended in 500 µL of phosphate buffered saline (PBS) 0.04 M pH 7.2 and used to evaluate the oocyst viability. All tests were performed in duplicate.

2.3. Kinetic modeling

Kinetic parameters were estimated using different datasets obtained for the different submodels after replicated experiments: i) dark thermal inactivation; ii) UV irradiance effect; iii) UV radiation-temperature synergistic effect; and, iv) wavelength-dependent spectral action.

2.3.1. Dark thermal inactivation

Experimental data of inactivation in the dark were fitted to a first-order kinetic model (Eq. (1) and Eq. (2)):

$$\frac{dC}{dt} = -k_T \cdot C \tag{1}$$

$$\ln\left(\frac{C}{C_0}\right) = -k_T \cdot t \tag{2}$$

where C_0 is the initial concentration of the *C. parvum* (oocysts·mL^{-1}), C is the concentration at a specific time t, and k_T is the thermal inactivation kinetic constant.

The effect of the water temperature (T) on the thermal inactivation kinetic constant (k_T) was modeled by the Arrhenius equation (Arrhenius, 1889) with a threshold temperature (Eq. (3)):

$$k_T = k_{T_0} \cdot \exp\left(-\frac{E_{a_T}}{R} \cdot \left(\frac{1}{T} - \frac{1}{T_0}\right)\right) \tag{3}$$

where k_{T_0} is the temperature-independent pre-exponential factor, E_{a_T} is the activation energy, R is the universal gas constant, and T_0 is the threshold temperature. As Peleg et al. (2012) demonstrated, the threshold temperature can be suppressed, which involves a different value of k_{T_0} for the same value of k_T. However, the present model kept the T_0 as a conceptual threshold to account for the temperature above which the thermal effect is observed. The kinetic parameters of the model (k_{T_0} and E_{a_T}/R) have been calculated by minimizing the normalized root mean square error (NRMSE) between the predicted and observed concentration of viable *C. parvum* oocysts using a constrained nonlinear multivariable optimization algorithm employing the add-in Solver of Excel 2016 software (Microsoft® Corp., Redmond, Washington, USA).

2.3.2. UV irradiance effect

The presence of a shoulder in the experimental photoinactivation curves suggests the application of a series-event kinetic model (Severin et al., 1983) to reproduce the experimental data. This model assumes that an event is a unit of damage, and n units of damage must be accumulated to inactivate the microorganisms. Therefore, the inactivation process takes place through a sequence of inactivation levels (n). In the population balance of microorganisms at level i ($1 \le i \le n$), the damaged organisms from the previous level are considered as a source (positive term) and the damaged organisms at the current level are considered as a sink (negative term). This balance is represented by Eq. 4:

$$\frac{dC_i}{dt} = k_{RAD} \cdot I \cdot C_{i-1} - k_{RAD} \cdot I \cdot C_i \tag{4}$$

where C_i is the concentration of viable *C. parvum* oocysts (oocysts·mL^{-1}) at level i at a specific time t, C_{i-1} is the concentration of viable *C. parvum* oocysts (oocysts·mL^{-1}) at the previous level, k_{RAD} is the photoinactivation constant, and I is the UV irradiance (W·m^{-2}). The values of n and k_{RAD} were calculated minimizing the normalized root mean square logarithmic error (NRMSLE) between experimental and predicted concentrations of viable *C. parvum* oocysts over time in experiments without thermal effect (30 °C of water temperature) using a constrained nonlinear multivariable optimization algorithm employing the add-in Solver of Excel 2016 software (Microsoft® Corp.).

2.3.3. UV radiation-temperature synergistic effect

To account for this synergistic effect in the model, k_{RAD} from Eq. (4) was redefined with the Arrhenius equation (Eq. (5)):

$$k_{RAD} = k_{RAD_0} \cdot \exp\left(-\frac{E_{a_{RAD}}}{R} \cdot \left(\frac{1}{T} - \frac{1}{T_0}\right)\right) \tag{5}$$

where k_{RAD_0} is the temperature-independent pre-exponential factor, and $E_{a_{RAD}}$ is the activation energy. The kinetic parameters of the model (k_{RAD_0}, $E_{a_{RAD}}/R$, n, k_{T_0} and E_{a_T}/R) were recalculated minimizing the NRMSLE between the predicted and observed values of the kinetic constants, using the sequential quadratic programming (SQP) nonlinear optimization tool implemented in GNU Octave platform (www.octave.org). The values of the kinetic parameters previously calculated in the previous submodels were used as seeds for the optimization.

2.3.4. Wavelength-dependent spectral action

Finally, to describe *C. parvum* sensitivity to solar inactivation as a function of wavelength, a quantum yield ϕ_{CP} was defined as the ratio between the number of damaged oocysts and the number of absorbed photons. To determine the rate of photon absorption, the absorption spectrum for a single oocyst was defined like Mattle et al. (2015) previously did for adenovirus, MS2, and phiX174 viruses. As Busse et al. (2019) demonstrated, absorption of solar light by *C. parvum* is dominated by the nucleic acid components, since the action spectrum is similar in shape to the DNA absorption spectrum, with a maximum around 260 nm. The absorbance at 260 nm can be calculated by multiplying the weight of dsDNA in *C. parvum* by the weight-normalized extinction coefficient of the dsDNA at 260 nm, $\varepsilon_{CP}(260nm)$, reported as 0.020 mL·µg^{-1}·cm^{-1} (Gallagher, 2011). The weight of the DNA of *C. parvum* was calculated following data deposited in National Center for Biotechnology Information (NCBI, Reference CM000429.1) (National Center for Biotechnology Information, 2020) and corresponds to 9.51 × 10^{-10} µg. The absorption spectrum for *C. parvum* was determined by considering the shape of the absorption spectrum of a *C. parvum* oocyst suspension measured by Busse et al. (2019) and kindly provided by the authors upon request. A 5-point smoothing was applied to the spectrum data in the range from 240 to 400 nm, and the values were normalized to the absorption at 260 nm. The final results of the spectral extinction coefficients of a single *C. parvum* oocyst, $\varepsilon_{CP}(\lambda)$ (mL·oocyst^{-1}cm^{-1}) are shown in Table S2.

As a result, the photoinactivation kinetic parameter can be expressed according to Eq. (6):

$$k_{RAD0} \cdot I = \phi_{CP} \cdot \int_{\lambda} \varepsilon_{CP}(\lambda) \cdot I(\lambda) \cdot \frac{\lambda}{h \cdot c} \cdot d\lambda \tag{6}$$

where $\frac{\lambda}{h \cdot c}$ (photon·J^{-1}) converts the energy units of the spectral irradiance, $I(\lambda)$, to the photonic units, where h is the Planck's constant and c is the speed of light in vacuum. The value of the quantum yield, ϕ_{CP}, can be calculated by resolution of Eq. (6).

3. Results and discussion

3.1. Dark thermal inactivation

Data from experiments in dark conditions were evaluated at water temperatures commonly achieved during solar exposure of water (30, 40, 42, 43, 44, and 45 °C). Experimental results shown in Fig. S1 confirm a noticeable effect of temperature, the experiment at 30 °C being the only case in which inactivation did not happen. For this reason, the threshold temperature of the Arrhenius equation (T_0 in Eq. (3)) was set to 30 °C (303 K). The experimental results (two replicates in all cases) were fitted to a first-order kinetic model (Eq. (1)), and the values of the kinetic constant

were used to calculate the provisional values of the thermal kinetic parameters ($k_{T_0} = 1.12 \times 10^{-4}$ h^{-1} and $E_{a_T}/R = 4.37 \times 10^5$ K, NRMSE = 8.59%). These parameters will be refined later with the complete set of experimental data, using these provisional values as seeds. Predicted results of the thermal inactivation are also shown in Fig. S1.

Some reports found no effects on *C. parvum* survival for water temperatures up to 40 °C (Liu et al., 2015). However, other publications suggested that the viability of *C. parvum* decreases progressively for temperatures in the range from 30 to 50 °C due to the melting point of the fatty acids and hydrocarbons present in the oocyst wall and the increase in the metabolic activity (Fayer and Nerad, 1996; Jenkins et al., 2010; King et al., 2005; Peng et al., 2008). Furthermore, temperatures above 37 °C can induce the phenomenon of spontaneous excystation of *C. parvum* oocysts, making their survival impossible in the absence of a host (Gómez-Couso et al., 2009; Smith et al., 2005). However, these phenomena do not necessarily follow a pure Arrhenius behavior, what can explain the small deviations observed in experiments at 40 and 42 °C.

3.2. UV irradiance effect

Data from *C. parvum* inactivation experiments under illumination (UV irradiance of 30, 40, and 50 W·m^{-2}) at a temperature of 30 °C to neglect thermal effects were fitted to a series-event model (Eq. (4)). Calculation of the kinetic parameters ($n = 8$ and $k_{RAD} = 4.05 \times 10^{-2}$ m^2·W^{-1}·h^{-1}) was carried out by fitting the experimental data with an NRMSLE of 2.44% (see Fig. S2.1). The direct coupling of the dark thermal inactivation model with the UV irradiance model failed to predict the inactivation of *C. parvum* at temperatures higher than 30 °C (Figs. S2.2 and S2.3) with a global value of NRMSLE = 17.9%. The predictions clearly underestimate the experimental data, showing a higher error for higher temperatures, which supports the existence of a synergy between the thermal and photonic inactivation processes. The existence of a strong synergistic effect between the optical and thermal processes to inactivate microorganisms is well known (McGuigan et al., 1998; Wegelin et al., 1994) and has been modeled for bacteria and viruses (Castro-Alférez et al., 2017; García-Gil et al., 2020b).

3.3. UV radiation-temperature synergistic effect

The synergistic effect was included in the model through the temperature dependence of the kinetic constant of the series-event model according to the modified Arrhenius equation, using again a value of 30 °C (303 K) for the temperature threshold (T_0). All the kinetic parameters were recalculated using as seeds the provisional values in the previous submodels. The global fitting of the whole experimental data set for the complete range of irradiances and temperatures provides the values of the final kinetic parameters: $n = 7$, $k_{RAD0} = 2.97 \times 10^{-2}$ m^2·W^{-1}·h^{-1}, $E_{a_{RAD}}/R = 6.90 \times 10^4$ K, $k_{T_0} = 4.19 \times 10^{-5}$ h^{-1}, and $E_{a_T}/R = 5.06 \times 10^5$ K with an NRMSLE of 3.68% (Figs. 1.1, 1.2, 1.3, and 1.4). In this case, whereas the predictions of the dark thermal inactivation and the photoinactivation at 30 °C are very similar, the prediction of the photoinactivation at higher temperatures improves significantly.

3.4. Wavelength-dependent spectral action

The developed model, which considers the synergistic effect between the UV irradiance and temperature and the independent thermal effect, succeeds in reproducing the *C. parvum* inactivation using a light source with the solar spectrum. However, for the same global UV irradiance, if the spectral distribution of the radiation changes, the effective damage can also dramatically change. The wavelength-dependent spectral contribution needs to be modeled to predict the inactivation in solar disinfection containers with different transmission spectra. As suggested by Mattle et al. (2015), the inactivation rate can be calculated by multiplying the quantum yield, the concentration of microorganisms, and the volumetric rate of photon absorption (calculated as the integration in wavelength of the spectral microorganism extinction coefficient by the spectral irradiance for each wavelength). Table S2 shows the *C. parvum* extinction coefficients ($\varepsilon_{CP}(\lambda)$) (calculated in this work) and the spectral irradiance ($I(\lambda)$) from 280 to 400 nm for a global UV (I) of 50 W·m^{-2}. Following Eq. (6), the quantum yield for *C. parvum* inactivation with the solar simulator spectrum was calculated as $\phi_{CP} = 3.94 \times 10^{-7}$ oocysts damaged per absorbed photon, indicating that *C. parvum* is more resistant to direct inactivation than viruses such as phiX174, MS2, and adenovirus (1.4×10^{-2}, 2.9×10^{-3}, and 2.5×10^{-4} virus in-

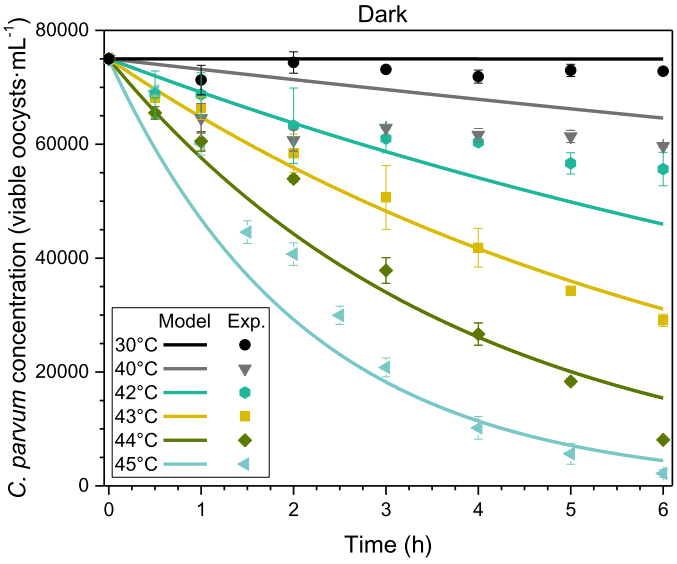

Fig. 1.1. Observed inactivation profiles of *C. parvum* oocysts in distilled water after exposure to different temperatures in dark conditions and predictions with the synergistic UV radiation-temperature model.

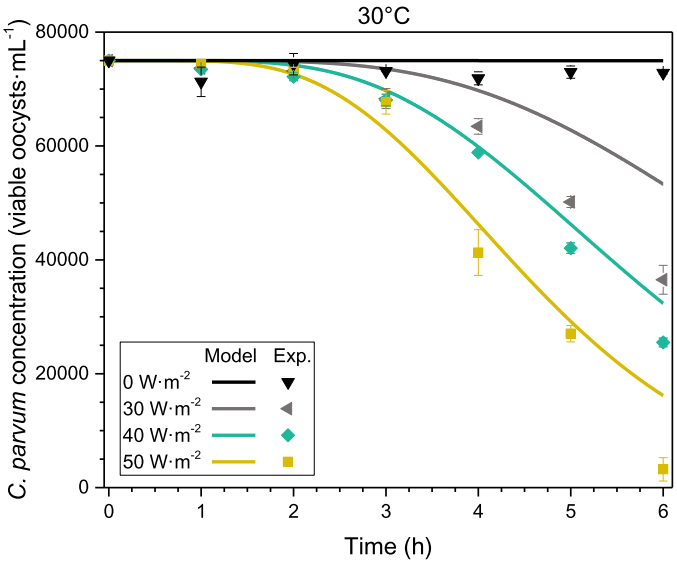

Fig. 1.2. Observed photoinactivation profiles of *C. parvum* oocysts in distilled water after exposure at 30 °C to different intensities of solar radiation and predictions with the synergistic UV radiation-temperature model.

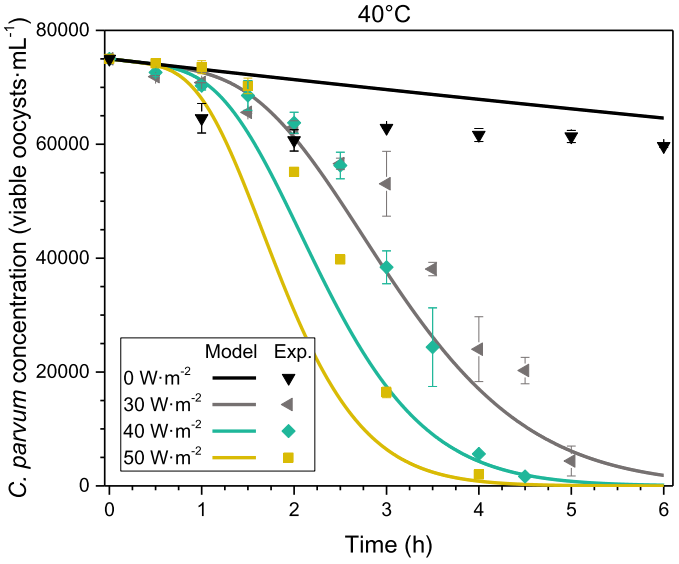

Fig. 1.3. Observed photoinactivation profiles of *C. parvum* oocysts in distilled water after exposure at 40 °C to different intensities of solar radiation and predictions with the synergistic UV radiation-temperature model.

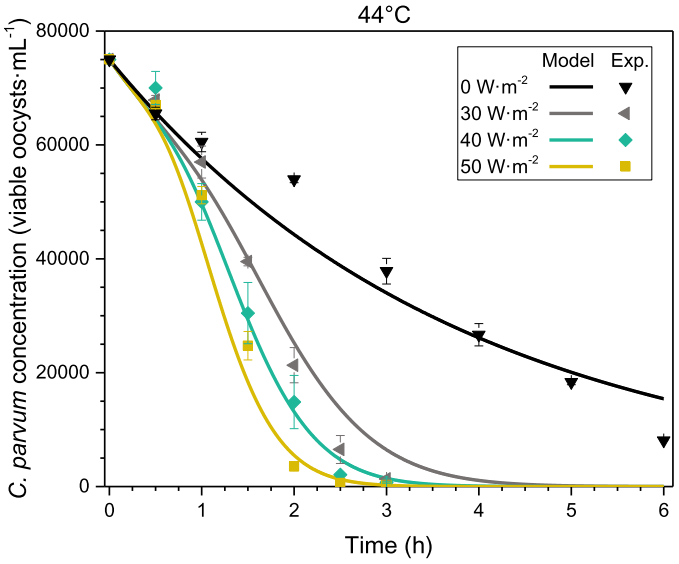

Fig. 1.4. Observed photoinactivation profiles of *C. parvum* oocysts in distilled water after exposure at 44 °C to different intensities of solar radiation and predictions with the synergistic UV radiation-temperature model.

activated per absorbed photon, respectively) (Mattle et al., 2015). In any case, it is important to notice the critical role of the calibration of the spectroradiometer used to measure the emission of the incident radiation, especially in the UVB range. For instance, in the case of the MS2 virus different values of the quantum yield can be found in the literature: 2.07×10^{-3}, 2.9×10^{-3} and 2.56×10^{-4} viruses inactivated per absorbed photon for García-Gil et al. (2020b), Mattle et al. (2015) and Silverman et al. (2019), respectively. The reason for these apparent discrepancies is the high sensibility of the results to the experimental data provided by the spectroradiometer. Basically, each quantum yield value worked well in the framework of the spectral measurements from which it was derived. In this sense, the use of quantum yields reported in the literature should be carefully selected and the calculation for each specific device is always recommended.

3.5. Validation of the model

The developed model is able to predict the inactivation of *C. parvum* oocysts depending on the water temperature, irradiance, and spectral distribution of the incident light, allowing the estimation of the required inactivation times for different locations around the world. Additionally, the model has also a particular strength: the capability of estimating required solar exposure time when solar water disinfection is performed in containers made of any material with a known transmission spectrum. To validate this strength, experiments were carried out using plastic materials of different UV-B transmittance: PET, PP, and PMMA and combining two levels of global UV irradiance (30 and 50 $W \cdot m^{-2}$) and water temperature (30 and 44 °C) in three experiments (the experiment with the lowest values of both variables was neglected). Figs. 2.1, 2.2, and 2.3 show the comparison between the observed and the predicted inactivation profiles of *C. parvum* oocysts *versus* the exposure time for the PET, PP, and PMMA scenarios. Considering the fully predictive nature of the model inactivation curves (they are not fitting results), the agreement can be considered very good, with values of NRMSLE of 5.54, 5.72, and 11.68% for PET, PP, and PMMA, respectively. The results can be easily interpreted based on the different UV transmission of the materials: 1%, 44%, and 57% in the global UV-B range, and 59%, 60%, and 86% in the UV-A range, for PET, PP, and PMMA, respectively. The radiation transmitted and the *C. parvum* extinction coefficients *versus* wavelength are shown in Fig. 3 (data in Table S2). As can be observed, the UV-B is the critical region in which the *C. parvum* absorption mainly overlaps with the spectrum of the incident radiation, and therefore the UV-B transmission will be very significant in the *C. parvum* photoinactivation. However, as shown Fig. 3, the emission of the solar simulator overestimates the irradiance of the standard AM 1.5 solar spectrum, especially in the 280–300 nm range where the process is very sensitive. Consequently, under real sunlight, PP and PMMA would be expected to perform slightly worse. For the PP and PMMA scenarios, the photoinactivation is possible being higher for the plastic with the higher transmission (PMMA). The thermal effect and the irradiance effect can be observed in both cases for experiments at the same global UV irradiance and the same water temperature, respectively. In the case of PET, plastic that essentially does not transmit UV-B radiation, the thermal contribution is almost the only damage source in pure water, achieving at simple sight the same disinfection rate for different values of global UV irradiance (model predictions for 30 and 50 $W \cdot m^{-2}$ at 44 °C seem to be the same). The type of photodamage can be direct or indirect (Nelson et al., 2018). Direct damage is due to the absorption of radiation by genome (DNA in this case) and is mainly initiated by photons in the UV-B range. The indirect damage is caused when an external or internal photosensitizer, that can absorb UV-B radiation as well as UV-A and visible radiation, produces photo-produced reactive intermediates (PPRI) that damage the microorganisms (*i.e.* reactive oxidative species (ROS)) (Nelson et al., 2018). The absence of external sensitizers (experiments carried out in distillate water) and the negligible inactivation with only UV-A and visible radiation at low temperature (PET scenario at 30 °C) leads to think that *C. parvum* cannot be damage by endogenous indirect damage produced by internal photosensitizers. However, King et al., 2010 were unable to readily detect cyclobutane pyrimidine dimers formation or DNA damage in oocysts exhibiting similar or greater levels of inactivation by solar UV but they proved that solar UV radiation induces sporozoite membrane depolarization, resulting in reduced cellular ATP and increased cytosolic calcium, accompanied by a reduction in the internal granularity of sporozoites, indicative of apical organelle discharge and sporozoite exocytosis, resulting in a significant reduction in the ability of sporozoites to attach and invade host cells.

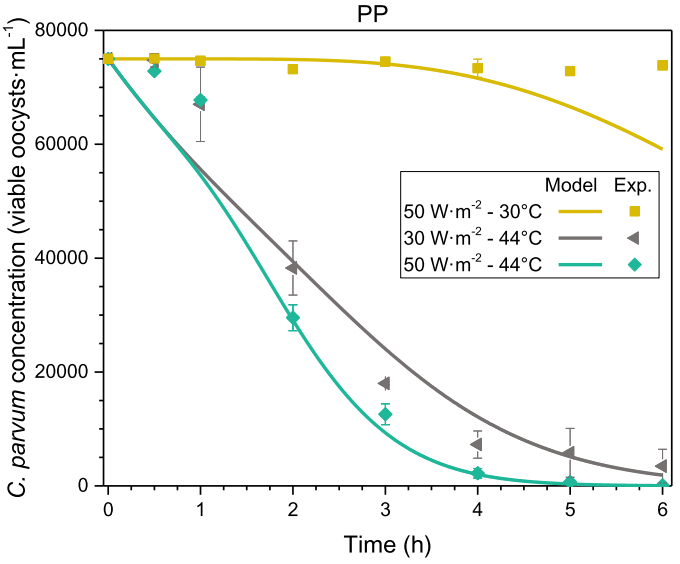

Fig. 2.1. Observed and predicted inactivation profiles of *C. parvum* oocysts in distilled water after exposure at different combinations of intensities of solar radiation and temperatures during the experiments of validation using polypropylene (PP) to modify the spectral distribution of radiation.

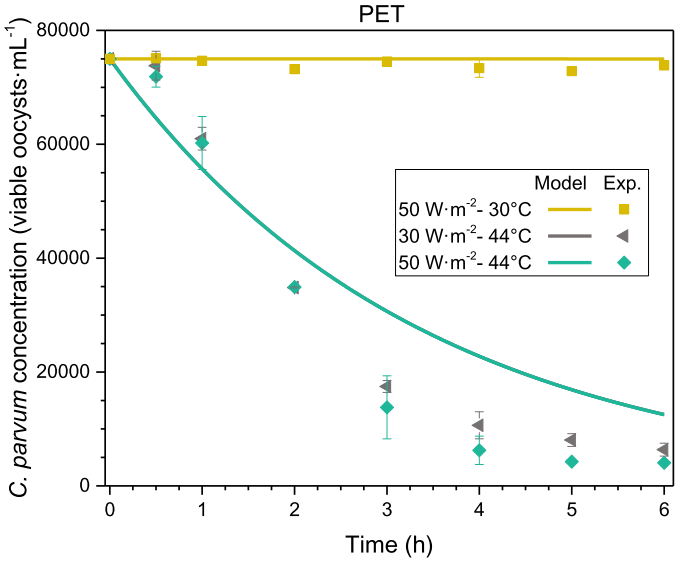

Fig. 2.3. Observed and predicted inactivation profiles of *C. parvum* oocysts in distilled water after exposure at different combinations of intensities of solar radiation and temperatures during the experiments of validation using polyethylene terephthalate (PET) to modify the spectral distribution of radiation. Prediction profiles for 44 °C are practically equal (gray and blue lines).

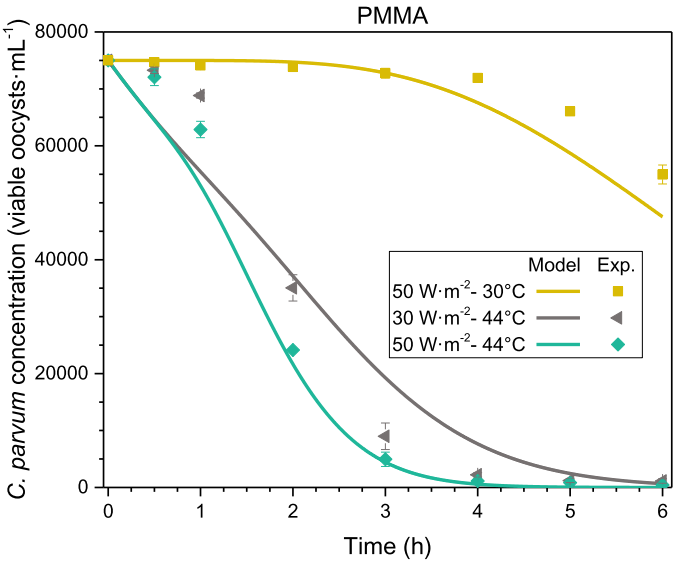

Fig. 2.2. Observed and predicted inactivation profiles of *C. parvum* oocysts in distilled water after exposure at different combinations of intensities of solar radiation and temperatures during the experiments of validation using polymethylmethacrylate (PMMA) to modify the spectral distribution of radiation.

Other authors confirm that the presence of natural organic matter (NOM), one of the known photosensitizers, did not improve the inactivation, likely due to the resistance of the thick oocyst wall to exogenous inactivation (Liu et al., 2015). Furthermore, in the case of using high volume containers, the damage produced by the external PPRI can be completely overshadowed by the role of the sensitizers as attenuators of radiation (García-Gil et al., 2020c). Moreover, only for the temperature higher than 30 °C, the thermal effect is noticeable. These facts confirm two things: the threshold on the thermal inactivation set to 30 °C and the dominant mechanism of *C. parvum* photoinactivation by the direct damage caused by the UV-B photons' absorption by DNA. Thus, it also means that the solar water disinfection of *C. parvum* in common containers of PET with pure water is practically possible because of thermal inactivation, however, reached temperature during solar water disinfection easily rises up to 30 °C (Dejung et al., 2007; Gómez-Couso et al., 2010).

In the present study, the survival of *C. parvum* oocysts were determined by the inclusion/exclusion of the fluorogenic vital dye PI, an indicator of the integrity and permeability of the oocyst wall (Campbell et al., 1992) which may be affected during SODIS procedures (McGuigan et al., 2006). This staining method is quick, simple, non-expensive and provides useful information in studies on the influence of environmental factors/pressures, as the temperature and radiation, on the survival of *Cryptosporidium* spp. oocysts. However, this technique overestimates the oocyst infectivity in comparison with cell culture methods and bioassays in murine models (Adeyemo et al., 2018; Robertson and Gjerde, 2007) providing a safety margin in the water treatment by SODIS, which will benefit the microbiological quality of the treated water and in protecting consumer health.

Moreover, it should be considered that in those geographical regions where the WHO recommends the use of SODIS as an alternative method of disinfection to guarantee the safety of water destined for human consumption, the levels of water turbidity varied widely. Depending on weather conditions and time of collection, the turbidity of water in some areas can vary between 5 and 2000 NTU daily (Joyce et al., 1996). Laboratory experiments have shown that in water samples of turbidity higher than 200 NTU, less than 1% of the total incident ultraviolet light (UV) penetrates further than a depth of 2 cm from the surface (Joyce et al., 1996). In this case, the role of temperature in the inactivation of *C. parvum* oocysts is more crucial and, therefore, the viability values determined by the inclusion/exclusion of fluorogenic vital dyes will be very similar to the infectivity values detected using a murine model or a cell culture.

Also, in a previous study in which the combined effects of solar radiation intensity, water turbidity and exposure time on the survival of *C. parvum* oocysts during simulated SODIS exposure were investigated, it was showed that only in those cases in which the infectivity was not 100%, the values of oocyst viability obtained by the inclusion/exclusion of PI were slightly higher than the

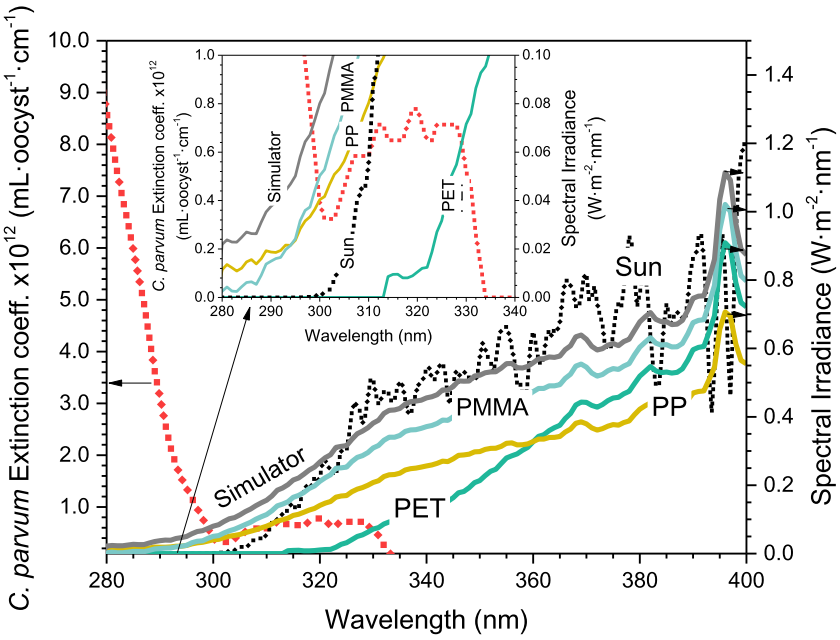

Fig. 3. Extinction coefficient of *C. parvum* (left axis) and spectral irradiance of the solar simulator and transmitted by PMMA, PP, and PET plastics (right axis). Inset: Details of the UV-B region.

corresponding values obtained with a neonatal murine model (Gómez-Couso et al., 2009).

4. Conclusions

A novel comprehensive kinetic model for the inactivation of *C. parvum* in clear water by solar light has been developed. The model considers the solar irradiance, water temperature, the photonic-thermal synergistic effect, and the specific sensibility of *C. parvum* to the spectral distribution of radiation. A threshold temperature of 30 °C is considered in the model for the dark thermal inactivation of *C. parvum*, being this process especially significant above 40 °C. UV radiation also leads to the inactivation, being the efficacy strongly affected by the spectral distribution of the incident light, as *C. parvum* inactivation in mainly driven by photons in the UV-B range. The quantum yield of the photonic process has been calculated from experimental data and the spectral extinction coefficients of *C. parvum* has been also determined. These values reflect the strong sensitivity of the process to the spectral distribution of the incident light, in agreement with the biological mechanism of *Cryptosporidium* oocyst inactivation based on the direct absorption of photons by the nucleic acids. The joint action of temperature and radiation leads to a strong synergistic effect that improves the efficacy of the process. The incorporation of this synergistic effect in the model gives very meaningful predictions with an average fitting error of the experimental data of only 3.7%.

Finally, the predictions of this comprehensive model have been successfully validated with experimental data from three different scenarios of variable temperature and spectral transmission in the UV range. Predictions of solar inactivation using PET, PP, and PMMA materials led to errors of 5.5, 5.7, and 11.7%, respectively. Therefore, the developed model constitutes a powerful tool for the predictive evaluation of *C. parvum* inactivation rate under different solar spectral irradiance and environmental temperature conditions for any location worldwide. Applications range from the estimation of the natural inactivation in the environment to the technical design of solar water disinfection processes for drinking water supply, including the spectral transmission of the materials. However, because SODIS procedures can be implemented in different geographical regions, it is recommended to carry out experiments in order to adjust the model to local conditions.

Supplementary Information

Experimental data and predictions for dark thermal inactivation; experimental data and predictions for the thermal-radiation additive model; spectral extinction coefficients of *C. parvum*; spectral emission from the solar simulator and transmitted radiation through sheets of different plastics materials.

Declaration of Competing Interest

The authors declare that they have no known competing financial interests or personal relationships that could have appeared to influence the work reported in this paper.

Acknowledgments

The authors gratefully acknowledge the financial support of the European Union's Horizon 2020 research and innovation program under WATERSPOUTT H2020-Water-5c-2015 project (GA 688928) and under PANIWATER project (GA 820718), jointly funded by the European Commission and the Department of Science and Technology of India (DST). Ángela García Gil also acknowledges Técnicas Reunidas for the economic support to finance her scholarship in Residencia de Estudiantes and Spanish Ministry of Education for her FPU grant (FPU17/04333). The authors would like to thank the glass-blowing staff of the RIAIDT-USC for technical advice and Mr. Martin Vincent and Dr. Tracy Morse for the supply of the PMMA and PP plastic materials. The authors also thank Prof Ernest R. Blatchley III for the supply of the experimental data of the absorption spectrum of DNA of *C. parvum*.

Supplementary materials

Supplementary material associated with this article can be found, in the online version, at doi:10.1016/j.watres.2020.116226.

References

Adeyemo, F.E., Singh, G., Reddy, P., Stenström, T.A., 2018. Methods for the detection of *Cryptosporidium* and *Giardia*: from microscopy to nucleic acid based tools in clinical and environmental regimes. Acta Trop. 10.1016/j.actatropica.2018.01.011

Abeywardena, H., Jex, A.R., Gasser, R.B., 2015. A perspective on *Cryptosporidium* and *Giardia*, with an emphasis on bovines and recent epidemiological findings. Adv. Parasitol 88, 243–301. doi:10.1016/bs.apar.2015.02.001.

Arrhenius, S., 1889. Über die Reaktionsgeschwindigkeit bei der Inversion von Rohrzucker durch Säuren. Zeitschrift für Phys. Chemie 4. doi:10.1515/zpch-1889-0116.

Beck, S.E., Wright, H.B., Hargy, T.M., Larason, T.C., Linden, K.G., 2015. Action spectra for validation of pathogen disinfection in medium-pressure ultraviolet (UV) systems. Water Res. 70, 27–37. doi:10.1016/j.watres.2014.11.028.

Betancourt, W.Q., Rose, J.B., 2004. Drinking water treatment processes for removal of *Cryptosporidium* and *Giardia*. Vet. Parasitol. 126, 219–234. doi:10.1016/j.vetpar.2004.09.002.

Busse, M.M., Becker, M., Applegate, B.M., Camp, J.W., Blatchley, E.R., 2019. Responses of *Salmonella typhimurium* LT2, *Vibrio harveyi*, and *Cryptosporidium parvum* to UVB and UVA radiation. Chem. Eng. J. 10.1016/j.cej.2019.04.105

Cacciò, S.M., Putignani, L., 2014. Epidemiology of human cryptosporidiosis. In: *Cryptosporidium*: parasite and Disease. Springer-Verlag, Wien, pp. 43–79. doi:10.1007/978-3-7091-1562-6_2.

Campbell, A.T., Robertson, L.J., Smith, H.V., 1992. Viability of *Cryptosporidium parvum* oocysts: correlation of *in vitro* excystation with inclusion or exclusion of fluorogenic vital dyes. Appl. Environ. Microbiol. 58, 3488–3493. doi:10.1128/aem.58.11.3488-3493.1992.

Castro-Alférez, M., Polo-López, M.I., Marugán, J., Fernández-Ibáñez, P., 2017. Mechanistic modeling of UV and mild-heat synergistic effect on solar water disinfection. Chem. Eng. J. 316, 111–120. doi:10.1016/j.cej.2017.01.026.

Dejung, S., Fuentes, I., Almanza, G., Jarro, R., Navarro, L., Arias, G., Urquieta, E., Torrico, A., Fenandez, W., Iriarte, M., Birrer, C., Stahel, W.A., Wegelin, M., 2007. Effect of solar water disinfection (SODIS) on model microorganisms under improved and field SODIS conditions. J. Water Supply Res. Technol. - AQUA 56, 245–256. doi:10.2166/aqua.2007.058.

Dowd, S.E., Pillai, S.D., 1997. A rapid viability assay for *Cryptosporidium* oocysts and *Giardia* cysts for use in conjunction with indirect fluorescent antibody detection. Can. J. Microbiol. 43, 658–662. doi:10.1139/m97-093.

Efstratiou, A., Ongerth, J.E., Karanis, P., 2017. Waterborne transmission of protozoan parasites: review of worldwide outbreaks - An update 2011–2016. Water Res. 114, 14–22. doi:10.1016/j.watres.2017.01.036.

Fayer, R., Nerad, T., 1996. Effects of low temperatures on viability of *Cryptosporidium* parvum oocysts. Appl. Environ. Microbiol. 62, 1431.

Gallagher, S.R., 2011. Quantitation of DNA and RNA with absorption and fluorescence spectroscopy. Curr. Protoc. Mol. Biol. 93, 1–14. doi:10.1002/0471142727.mba03ds93.

García-Gil, Á., Martinez, A., Polo-López, M.I., Marugán, J., 2020a. Kinetic modeling of the synergistic thermal and spectral actions on the inactivation of viruses in water by sunlight. Water Res. 116074. doi:10.1016/j.watres.2020.116074.

García-Gil, Á., Pablos, C., García-Muñoz, R.A., McGuigan, K.G., Marugán, J., 2020b. Material selection and prediction of solar irradiance in plastic containers for application of solar water disinfection (SODIS) to inactivate viruses, bacteria and protozoa. Sci. Total Environ. 730, 139126. doi:10.1016/j.scitotenv.2020.139126.

García-Gil, Á., Valverde, R., García-Muñoz, R.A., McGuigan, K.G., Marugán, J., 2020c. Solar Water Disinfection in high-volume containers: are naturally occurring substances attenuating factors of radiation? Chem. Eng. J. 339, 125852. doi:10.1016/j.cej.2020.125852.

Gómez-Couso, H., Fontán-Sainz, M., Ares-Mazás, E., 2010. Thermal contribution to the inactivation of *Cryptosporidium* in plastic bottles during solar water disinfection procedures. Am. J. Trop. Med. Hyg. 82, 35–39. doi:10.4269/ajtmh.2010.09-0284.

Gómez-Couso, H., Fontán-Sainz, M., Fernández-Alonso, J., Ares-Mazás, E., 2009. Excystation of *Cryptosporidium parvum* at temperatures that are reached during solar water disinfection. Parasitology 136, 393–399. doi:10.1017/S0031182009005563.

Gómez-Couso, H., Fontán-Sainz, M., Fernández-Ibáñez, P., Ares-Mazás, E., 2012. Speeding up the solar water disinfection process (SODIS) against *Cryptosporidium parvum* by using 2.5l static solar reactors fitted with compound parabolic concentrators (CPCs). Acta Trop. 124, 235–242. doi:10.1016/j.actatropica.2012.08.018.

Gómez-Couso, H., Fontán-Sainz, M., McGuigan, K.G., Ares-Mazás, E., 2009. Effect of the radiation intensity, water turbidity and exposure time on the survival of *Cryptosporidium* during simulated solar disinfection of drinking water. Acta Trop. 112, 43–48. doi:10.1016/j.actatropica.2009.06.004.

Gómez-Couso, H., Fontán-Sainz, M., Navntoft, C., Fernández-Ibáñez, P., Ares-Mazás, E., 2012. Comparison of different solar reactors for household disinfection of drinking water in developing countries: evaluation of their efficacy in relation to the waterborne enteropathogen *Cryptosporidium parvum*. Trans. R. Soc. Trop. Med. Hyg. 106, 645–652. doi:10.1016/j.trstmh.2012.07.014.

Hamilton, K.A., Waso, M., Reyneke, B., Saeidi, N., Levine, A., Lalancette, C., Besner, M.-C., Khan, W., Ahmed, W., 2018. *Cryptosporidium* and *Giardia* in wastewater and surface water environments. J. Environ. Qual. 47, 1006–1023. doi:10.2134/jeq2018.04.0132.

Hofstra, N., Vermeulen, L.C., 2016. Impacts of population growth, urbanisation and sanitation changes on global human *Cryptosporidium* emissions to surface water. Int. J. Hyg. Environ. Health 219, 599–605. doi:10.1016/j.ijheh.2016.06.005.

Jenkins, M.B., Eaglesham, B.S., Anthony, L.C., Kachlany, S.C., Bowman, D.D., Ghiorse, W.C., 2010. Significance of wall structure, macromolecular composition, and surface polymers to the survival and transport of *Cryptosporidium parvum* oocysts. Appl. Environ. Microbiol. 76, 1926–1934. doi:10.1128/AEM.02295-09.

Joyce, T.M., McGuigan, K.G., Elmore-Meegan, M., Conroy, R.M., 1996. Inactivation of fecal bacteria in drinking water by solar heating. Appl. Environ. Microbiol. 62, 399–402.

Karanis, P., Kourenti, C., Smith, H., 2007. Waterborne transmission of protozoan parasites: a worldwide review of outbreaks and lessons learnt. J. Water Health 5, 1–38. doi:10.2166/wh.2006.002.

Kilani, R.T., Sekla, L., 1987. Purification of *Cryptosporidium* oocysts and sporozoites by cesium chloride and percoll gradients. Am. J. Trop. Med. Hyg. 36, 505–508. doi:10.4269/ajtmh.1987.36.505.

King, B.J., Hoefel, D., Ee Wong, P., Monis, P.T., 2010. Solar radiation induces non-nuclear perturbations and a false start to regulated exocytosis in *Cryptosporidium parvum*. PLoS ONE 5, e11773. doi:10.1371/journal.pone.0011773.

King, B.J., Keegan, A.R., Monis, P.T., Saint, C.P., 2005. Environmental temperature controls *Cryptosporidium* oocyst metabolic rate and associated retention of infectivity. Appl. Environ. Microbiol. 71, 3848–3857. doi:10.1128/AEM.71.7.3848-3857.2005.

Kotloff, K.L., Nataro, J.P., Blackwelder, W.C., Nasrin, D., Farag, T.H., Panchalingam, S., Wu, Y., Sow, S.O., Sur, D., Breiman, R.F., Faruque, A.S.G., Zaidi, A.K.M., Saha, D., Alonso, P.L., Tamboura, B., Sanogo, D., Onwuchekwa, U., Manna, B., Ramamurthy, T., Kanungo, S., Ochieng, J.B., Omore, R., Oundo, J.O., Hossain, A., Das, S.K., Ahmed, S., Qureshi, S., Quadri, F., Adegbola, R.A., Antonio, M., Hossain, M.J., Akinsola, A., Mandomando, I., Nhampossa, T., Acácio, S., Biswas, K., O'Reilly, C.E., Mintz, E.D., Berkeley, L.Y., Muhsen, K., Sommerfelt, H., Robins-Browne, R.M., Levine, M.M., 2013. Burden and aetiology of diarrhoeal disease in infants and young children in developing countries (the Global Enteric Multicenter Study, GEMS): a prospective, case-control study. Lancet 382, 209–222. doi:10.1016/S0140-6736(13)60844-2.

Linden, K.G., Shin, G., Sobsey, M.D., 2001. Comparative effectiveness of UV wavelengths for the inactivation of *Cryptosporidium parvum* oocysts in water. Water Sci. Technol. 43, 171–174. doi:10.2166/wst.2001.0731.

Liu, Y., Dong, S., Kuhlenschmidt, M.S., Kuhlenschmidt, T.B., Drnevich, J., Nguyen, T.H., 2015. Inactivation mechanisms of *Cryptosporidium parvum* oocysts by solar ultraviolet irradiation. Environ. Sci. Water Res. Technol. 1, 188–198. doi:10.1039/c4ew00079j.

Lorenzo-Lorenzo, M.J., Ares-Mazas, M.E., de Maturana, I.V.-M., Duran-Oreiro, D., 1993. Effect of ultraviolet disinfection of drinking water on the viability of *Cryptosporidium parvum* oocysts. J. Parasitol. 79, 67–70. doi:10.2307/3283279.

Mattle, M.J., Vione, D., Kohn, T., 2015. Conceptual model and experimental framework to determine the contributions of direct and indirect photoreactions to the solar disinfection of MS2, phiX174, and adenovirus. Environ. Sci. Technol. 49, 334–342. doi:10.1021/es504764u.

McGuigan, K.G., Conroy, R.M., Mosler, H.-J., Preez, M.du, Ubomba-Jaswa, E., Fernandez-Ibañez, P., 2012. Solar water disinfection (SODIS): a review from bench-top to roof-top. J. Hazard. Mater. 235, 29–46. doi:10.1016/j.jhazmat.2012.07.053.

McGuigan, K.G., Joyce, T.M., Conroy, R.M., Gillespie, J.B., Elmore-Meegan, M., 1998. Solar disinfection of drinking water contained in transparent plastic bottles: characterizing the bacterial inactivation process. J. Appl. Microbiol. 84, 1138–1148. doi:10.1046/j.1365-2672.1998.00455.x.

McGuigan, K.G., Méndez-Hermida, F., Castro-Hermida, J.A., Ares-Mazás, E., Kehoe, S.C., Boyle, M., Sichel, C., Fernández-Ibáñez, P., Meyer, B.P., Ramalingham, S., Meyer, E.A., 2006. Batch solar disinfection inactivates oocysts of *Cryptosporidium parvum* and cysts of *Giardia muris* in drinking water. J. Appl. Microbiol. 101, 453–463. doi:10.1111/j.1365-2672.2006.02935.x.

Nasser, A.M., 2016. Removal of *Cryptosporidium* by wastewater treatment processes: a review. J. Water Health 14, 1–13. doi:10.2166/wh.2015.131.

National Center for Biotechnology Information [WWW Document], 2020. URL https://www.ncbi.nlm.nih.gov/ (accessed 3.16.20).

Nelson, K.L., Boehm, A.B., Davies-Colley, R.J., Dodd, M.C., Kohn, T., Linden, K.G., Liu, Y., Maraccini, P.A., McNeill, K., Mitch, W.A., Nguyen, T.H., Parker, K.M., Rodriguez, R.A., Sassoubre, L.M., Silverman, A.I., Wigginton, K.R., Zepp, R.G., 2018. Sunlight-mediated inactivation of health-relevant microorganisms in water: a review of mechanisms and modeling approaches. Environ. Sci. Process. Impacts 20, 1089–1122. doi:10.1039/c8em00047f.

Peleg, M., Normand, M.D., Corradini, M.G., 2012. The Arrhenius equation revisited. Crit. Rev. Food Sci. Nutr. 52, 830–851. doi:10.1080/10408398.2012.667460.

Peng, X., Murphy, T., Holden, N.M., 2008. Evaluation of the effect of temperature on the die-off rate for *Cryptosporidium parvum* oocysts in water, soils, and feces. Appl. Environ. Microbiol. doi:10.1128/AEM.01442-08.

Putignani, L., Menichella, D., 2010. Global distribution, public health and clinical impact of the protozoan pathogen *Cryptosporidium*. Interdiscip. Perspect. Infect. Dis. 2010, 1–39. doi:10.1155/2010/753512.

Robertson, L.J., Gjerde, B.K., 2007. *Cryptosporidium* oocysts: challenging adversaries? Trends Parasitol. 23, 344–347. doi:10.1016/j.pt.2007.06.002.

Ryan, U., Xiao, L., Read, C., Zhou, L., Lal, A.A., Pavlasek, I., 2003. Identification of novel *Cryptosporidium* genotypes from the Czech Republic. Appl. Environ. Microbiol. 69, 4302–4307. doi:10.1128/AEM.69.7.4302-4307.2003.

Severin, B.F., Suidan, M.T., Engelbrecht, R.S., 1983. Kinetic modeling of U.V. disinfection of water. Water Res. 17, 1669–1678. doi:10.1016/0043-1354(83)90027-1.

Silverman, A.I., Tay, N., Machairas, N., 2019. Comparison of biological weighting functions used to model endogenous sunlight inactivation rates of MS2 coliphage. Water Res. 151, 439–446. doi:10.1016/j.watres.2018.12.015.

Smith, H.V., Nichols, R.A.B., Grimason, A.M., 2005. *Cryptosporidium* excystation and invasion: getting to the guts of the matter. Trends Parasitol. doi:10.1016/j.pt.2005.01.007.

Sow, S.O., Muhsen, K., Nasrin, D., Blackwelder, W.C., Wu, Y., Farag, T.H., Panchalingam, S., Sur, D., Zaidi, A.K.M., Faruque, A.S.G., Saha, D., Adegbola, R., Alonso, P.L., Breiman, R.F., Bassat, Q., Tamboura, B., Sanogo, D., Onwuchekwa, U., Manna, B., Ramamurthy, T., Kanungo, S., Ahmed, S., Qureshi, S., Quadri, F., Hossain, A., Das, S.K., Antonio, M., Hossain, M.J., Mandomando, I., Nhampossa, T., Acácio, S., Omore, R., Oundo, J.O., Ochieng, J.B., Mintz, E.D., O'Reilly, C.E., Berkeley, L.Y., Livio, S., Tennant, S.M., Sommerfelt, H., Nataro, J.P., Ziv-Baran, T., Robins-Browne, R.M., Mishcherkin, V., Zhang, J., Liu, J., Houpt, E.R., Kotloff, K.L., Levine, M.M., 2016. The burden of *Cryptosporidium* diarrheal disease among children < 24 months of age in moderate/high mortality regions of Sub-Saharan Africa and South Asia, utilizing data from the Global Enteric Multicenter Study (GEMS). PLoS Negl. Trop. Dis. 10, e0004729. doi:10.1371/journal.pntd.0004729.

Swaffer, B., Abbott, H., King, B., van der Linden, L., Monis, P., 2018. Understanding human infectious *Cryptosporidium* risk in drinking water supply catchments. Water Res. 138, 282–292. doi:10.1016/j.watres.2018.03.063.

Vermeulen, L.C., van Hengel, M., Kroeze, C., Medema, G., Spanier, J.E., van Vliet, M.T.H., Hofstra, N., 2019. *Cryptosporidium* concentrations in rivers worldwide. Water Res. 149, 202–214. doi:10.1016/j.watres.2018.10.069.

Wegelin, M., Canonica, S., Mechsner, K., Fleischmann, T., Pesaro, F., Metzler, A., 1994. Solar water disinfection: scope of the process and analysis of radiation experiments. Aqua J. Water Supply Res. Technol. 43, 154–169.

WHO/UNICEF, 2005. Water for life: making it happen [WWW Document]. URL https://www.who.int/water_sanitation_health/monitoring/jmp2005/en/ (accessed 4.20.20).

WHO, 2015. WHO Estimates of the Global Burden of Diseases.